Optical and Quantum Electronics (2023) 55:625
https://doi.org/10.1007/s11082-023-04772-2

Modeling and investigation on the performance enhancement of hovering UAV-based FSO relay optical wireless communication systems under pointing errors and atmospheric turbulence effects

Mohammed R. Hayal[1] · Ebrahim E. Elsayed[1] · Dhiman Kakati[2] · Mehtab Singh[3] · Abdelrahman Elfikky[4] · Ayman I. Boghdady[5] · Amit Grover[6] · Shilpa Mehta[7] · Syed Agha Hassnain Mohsan[8] · Irfan Nurhidayat[9]

Received: 22 January 2023 / Accepted: 14 March 2023 / Published online: 18 May 2023
© The Author(s) 2023

Abstract
This paper investigates and enhances unmanned aerial vehicle (UAV) relay-assisted free-space optics (FSO) optical wireless communication (OWC) systems under the effects of pointing errors (PEs) and atmospheric turbulences (ATs). The incorporation of UAVs as buffer-aided moving relays in the conventional FSO (CFSO) relay-assisted systems is proposed for enhancing the performance of PEs through AT. Using M-PSK (phase shift keying) and M-QAM (quadrature amplitude modulation), the impact of PEs on transmission quality is evaluated in this work. We evaluate and optimize the symbol error rate, outage probability (OP), and signal-to-noise ratio (SNR) for the UAV-to-ground station-based FSO communications systems. The spatial diversity-based relay-assisted CFSO systems can enhance the performance of the UAV-UAV FSO links. In this paper, a new FSO (NFSO) channel model for the hovering UAV-FSO OWC fluctuations under the PEs, AT effects, jitter, deviation, receiving an error, and wind resistance effects are established. To improve the performance of hovering UAV-based FSO relay OWC systems. We reduce the influence of UAV-FSO OWC fluctuations under PEs and AT effects. By receiving incoherent signals at various locations, the spatial diversity-based relay-assisted NFSO systems can significantly increase the system's redundancy and enhance connection stability. Numerical results show that to achieve a bit-error-rate (BER) of $\leq 10^{-5}$, the required SNR is ≥ 23 dB when the wind variance of the UAVs σ_{α}^2 increases from 0 to 7 mrad with FSO link distance L = 2000 m. The required SNR is ≥ 25 dB when the wind variance σ_{α}^2 is 1 mrad at an OP of 10^{-6}. To obtain an average BER of 10^{-6}, the SNR should be 16.23 dB, 17.64 dB, and 21.45 dB when σ_{α}^2 is 0 mrad, 1 mrad, and 2 mrad, respectively. Using 8-PSK modulation without PEs requires 23.5 dB at BER of 10^{-8} while 16-QAM without PEs requires 26.5 dB to maintain the same BER of 10^{-8}. Compared with 16-QAM without PEs, the SNR gain of 8-PSK without PEs is 3 dB. The results show the relay-assisted UAV-FSO system with five stationary relays can achieve BER 10^{-8} at 25 dB SNR in the ideal case and 10^{-5} at 27 dB SNR with AT and PE at FSO length 1000 m. The results show the relay UAV-FSO system outperforms the CFSO at the BER and SNR performance. The effects of UAV'FSO s fluctuation increase when the UAV-FSO link length, L_{fso} increases. The results of the

Extended author information available on the last page of the article

weak turbulence achieve better SER compared with MT and ST. The obtained results show that decreasing L_{fso} can compensate for the effects of UAV-FSO link fluctuation on the proposed system. Finally, we investigated the CFSO relay-assisted UAV-FSO system with aided NFSO-UAVs spatial diversity-based relay-based on NFSO OWC and revealed the benefits of the resulting hybrid architecture.

Keywords Unmanned aerial vehicles (UAVs) · Free-space optics (FSO) communication link · Tilt angle · Pointing errors (PEs) · Atmospheric turbulence (AT) · UAV-FSO relay-assisted optical wireless communication systems

1 Introduction

The crucial advantages of free-space optics (FSO) communication technology, such as its high transmission capacity, extensive spectrum resources, superior confidentiality, and good directivity, have led to its widespread use in both the commercial and military sectors (Alzenad et al. 2018; Ghassemlooy et al. 2019; Khalighi and Uysal 2014). In addition, as unmanned aerial vehicles (UAVs) steadily expand from the military to the commercial and civil sectors, high-speed data transmission is frequently required in several specialized working environments, such as terrain survey and catastrophe detection. FSO communication technology is implemented in the field of UAV to provide high data rate optical network infrastructure in ground-to-ground and air-to-air scenarios (Khalighi and Uysal 2014). The FSO communication link between UAVs is essential for increasing their networking flexibility and coverage area. Recently, long-range wireless communications between two terrestrial stations have frequently been supported by UAVs and high-altitude platforms as relays (Michailidis et al. 2018; Fawaz et al. 2018). A depth discussion of the UAV FSO communication channel modeling can be found in Cruz and Fierro (2015); Dautov et al. 2018; Zheng et al. 2021). The use of wavelength division multiplexing (WDM) can expand transmission capabilities and applications for long-distance data transfer, hence increasing the optical wireless communication (OWC) capacity. High channel capacity is provided by dense-WDM (DWDM), which multiplexes several optical carrier signals into one communication channel (Yousif et al. 2019; Yousif and Elsayed 2019; Elsayed and Yousif 2020; Elsayed et al. 2018; Ciaramella et al. 2009). The most often used wavelength range for data transfers up to terabits per second is the optical C-band from (1530–1565 nm) (Ciaramella et al. 2009). FSO communication links are easy to deploy, high-bandwidth, cost-effective, license-free, and secure access technology (Zhang et al. 2021; Fotouhi et al. 2019; Elsayed et al. 2022). The front-hauling transfer of multimedia data collected by flying UAVs from the central position could be replaced by FSO communication (Alzenad et al. 2018; Zheng et al. 2021; Najafi et al. 2020; Kurt et al. 2021). However, the FSO link suffers from pressure and temperature fluctuations due to atmospheric turbulence (AT). FSO is additionally impacted by beam spreading losses, amplified spontaneous emission (ASE) noise, pointing errors (PEs), AT, misalignment, absorption, scattering, scintillation, inter-channel crosstalk (ICC), and power penalty (PP) (Yousif et al. 2019; Yousif and Elsayed 2019; Elsayed and Yousif 2020; Elsayed et al. 2018; Ciaramella et al. 2009). Techniques for minimizing ASE, AT, PP, ICC, and scintillation include adaptive multiple-input and multiple-output (MIMO) methods (Yousif et al. 2019; Yousif and Elsayed 2019; Elsayed and Yousif 2020) and wave-front sensor-based or sensorless adaptive optics systems. Recently, OWC systems and outdoor FSO systems have been developed and implemented with spatial modulation

(SM) diversity-based MIMO systems technology (Yousif et al. 2019; Yousif and Elsayed 2019). FSO systems employing DWDM with multiple channels support a greater capacity reach (32 channels × 40 Gbps) and are a simple way to enhance the data rate in the long-haul FSO data transfer (Yousif et al. 2019; Yousif and Elsayed 2019; Elsayed and Yousif 2020; Elsayed et al. 2018; Ciaramella et al. 2009). A closed-form statistical channel model has been proposed that takes into account such as the AT intensity, field angle, spatial information, PE variation, and transmit power. It requires a minimal set of UAV communication standard operations. To enhance communication quality, these parameters have been optimized (Zheng et al. 2021; Dabiri et al. 2018, 2019). A replaceable lens array has been used to modify the transmitter's beam divergence mechanism to increase the link's stability. (Dautov et al. 2018; Zheng et al. 2021). Previous studies focused on the communication between hovering UAVs and ignored the impact of instabilities and wind resistance. Only jitter and angle deviation will be affected by the UAV FSO communication in hovering modes (Najafi et al. 2020; Dabiri et al. 2018). In this paper, we analyze and investigate the performance enhancement of hovering UAV-based FSO relay optical wireless communication systems under PEs and AT effects. The proposed techniques for minimizing ASE, AT, PP, ICC, and scintillation using adaptive UAV-FSO MIMO methods and wave-front sensor-based or sensorless adaptive optics systems are investigated. In this paper, a new FSO (NFSO) communication channel model for the hovering UAV-FSO OWC fluctuations under the PEs, AT effects, jitter, deviation, receiving an error, and wind resistance effects are established. To improve the performance of hovering UAV-based FSO relay OWC systems. We reduce the influence of UAV-FSO OWC fluctuations under PEs and AT effects. By receiving incoherent signals at various locations, the spatial diversity-based relay-assisted NFSO systems can significantly increase the system's redundancy and enhance connection stability. We analyzed and derived the symbol error rate (SER) performance, taking into accounts such as link loss, transmitted power, total noise of the APD, various AT conditions, and PE loss. The rest of this article is structured as follows: Sect. 2 discusses the model and analysis of the UAV-FSO OWC communication system under the effects of PEs and AT. The SER is analyzed and derived in Sect. 3. The numerical results and discussion of the UAV-FSO communication link are presented in Sect. 4. This article is concluded in Sect. 5.

2 Analysis of UAV-FSO optical wireless communication link with pointing errors and atmospheric turbulence

When the UAV at the receiving end is flying horizontally, the arrival angle between the centerline of the beam and the receiving plane is not only influenced by the pointing deviation brought on by the jitter of the receiving end but also needs to take the tilt angle of the receiving plane into account (Zheng et al. 2021). Figure 1 shows the schematic diagram of the reception plane at the receiving end UAV which was reproduced from Zheng et al. (2021). The received signal at the receiving end of a wireless optical communication link can be expressed as (Zheng et al. 2021; Najafi et al. 2020):

$$y = hx + n \tag{1}$$

where n is the additive white Gaussian noise (AWGN), and x is the signal generated at the transmitting end. The following equation can provide h, the channel coefficient:

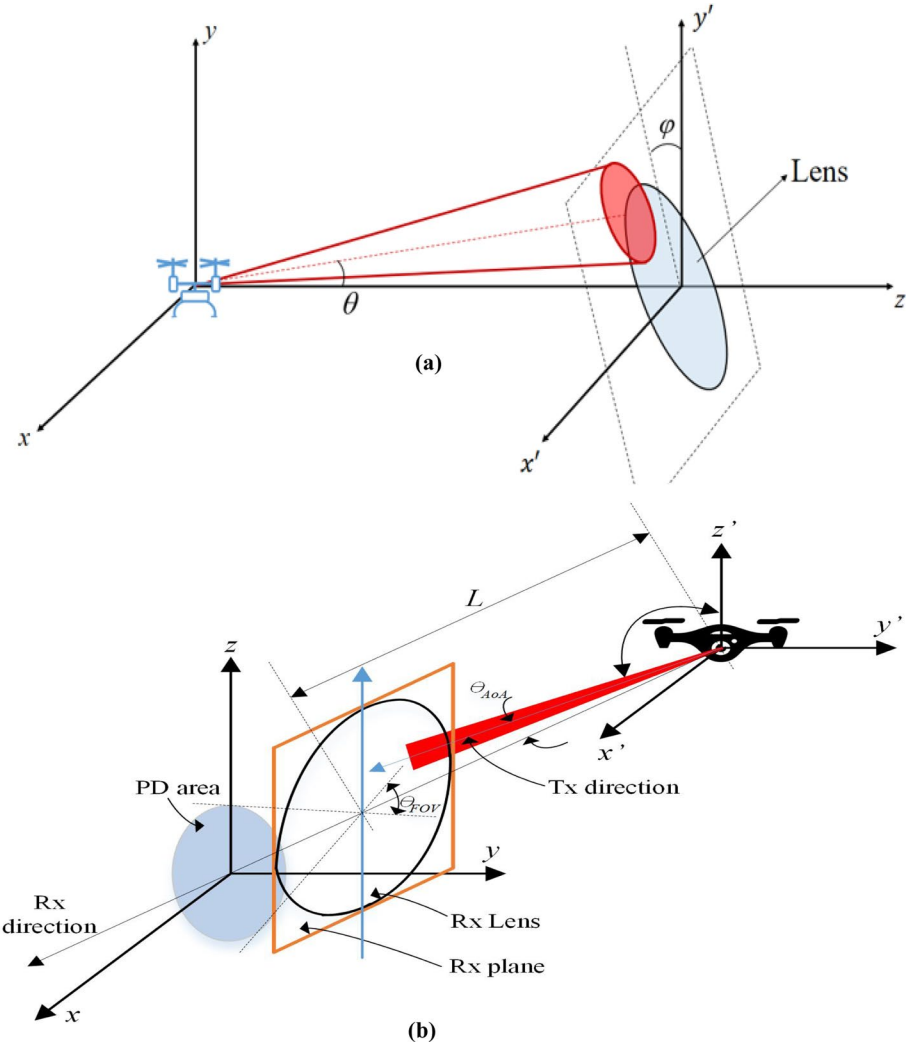

Fig. 1 System model at the 3D receiving plane end UAV-FSO relay-assisted free-space optical wireless systems for **a** FSO Tx (transmitter) and FSO receiver (RX) under the atmospheric turbulence effects reprinted from (Zheng et al. 2021), **b** for the received beam at the FSO Rx station under the atmospheric turbulence and pointing error in the presence of UAV-FSO fluctuations, reproduced from (Zheng et al. 2021; Trung 2021)

$$h = h_t h_a h_g \tag{2}$$

where h_t is the atmospheric channel's attenuation and AT coefficient for the position deviation of the transceiver in the hovering UAV-based FSO wireless communications and h_a represents the link interrupt coefficient, which denotes whether the spot is detected on the detection plane. h_g is the geometric and PE deviation coefficient, which denotes the position deviation between the spot center and the lens center at the receiving end. The Gamma-Gamma (GG) model and probability distribution function (PDF) of the log-normal (LN)

channels can be used to characterize the proposed system. The GG distribution of h_t in terms of the attenuation of the optical signal caused by air turbulence (Yousif et al. 2019; Yousif and Elsayed 2019; Elsayed and Yousif 2020; Elsayed et al. 2018; Andrews and Phillips 2012; Majumdar 2005; Khalighi et al. 2009; Aladeloba et al. 2012; Hayal et al. 2021):

$$f\left(\mathrm{h_t}\right) = \frac{2(\alpha\beta)^{\frac{(\alpha+\beta)}{2}}}{\Gamma(\alpha)\Gamma(\beta)}\mathrm{h_t}^{\left[\frac{\alpha+\beta}{2}\right]-1}\mathrm{K}_{\alpha-\beta}\left(2\sqrt{\alpha\beta\mathrm{h_t}}\right) \tag{3}$$

where $\Gamma(\cdot)$ is the Gamma function, $k_n(\cdot)$ is the nth order modified second kind of Bessel function. α and β indicate the effective numbers of the large-scale and small-scale eddies, respectively (Yousif et al. 2019; Yousif and Elsayed 2019; Elsayed and Yousif 2020; Elsayed et al. 2018; Andrews and Phillips 2012; Majumdar 2005; Khalighi et al. 2009; Aladeloba et al. 2012; Hayal et al. 2021):

$$\alpha = \left\{\exp\left[\frac{0.49\sigma_{\mathrm{R}}^2}{\left(1+1.11\sigma_{\mathrm{R}}^{\frac{12}{5}}\right)^{\frac{7}{6}}}\right]-1\right\}^{-1} \tag{4}$$

$$\beta = \left\{\exp\left[\frac{0.51\sigma_{\mathrm{R}}^2}{\left(1+0.69\sigma_{\mathrm{R}}^{\frac{12}{5}}\right)^{\frac{5}{6}}}\right]-1\right\}^{-1} \tag{5}$$

where the Rytov variance is expressed as:

$$\sigma_{\mathrm{R}}^2 = 1.23\mathrm{k}^{\frac{7}{6}}\mathrm{C}_{\mathrm{n}}^2\mathrm{L}^{\frac{11}{6}} \tag{6}$$

where k is the wave number, C_n^2 is the atmospheric refractive index structural (ARIS) parameter (Yousif et al. 2019; Yousif and Elsayed 2019; Elsayed and Yousif 2020; Elsayed et al. 2018; Andrews and Phillips 2012; Majumdar 2005; Khalighi et al. 2009; Aladeloba et al. 2012; Hayal et al. 2021), and L is the FSO distance (Yousif et al. 2019; Yousif and Elsayed 2019; Elsayed and Yousif 2020; Elsayed et al. 2018; Andrews and Phillips 2012; Majumdar 2005; Khalighi et al. 2009; Aladeloba et al. 2012; Hayal et al. 2021). The GG model's atmospheric turbulence is simulated in this work using the phase screen approach (Andrews and Phillips 2012; Majumdar 2005; Khalighi et al. 2009; Aladeloba et al. 2012; Hayal et al. 2021; Whitfield et al. 2012; Chatterjee and Mohamed 2014; Gudimetla et al. 2011). A small tilt will be present between the fuselage and the y-axis when a multi-rotor UAV is flying in a straight and horizontal trajectory, as seen in Fig. 1a (Zheng et al. 2021). The tilt angle influences the performance of the link through the coefficient h_a, which is related to the UAV's speed (Zheng et al. 2021). As seen in Fig. 1a, the included angle between the central axis and the y-axis is indicated as φ, assuming that the UAV at the receiving end is flying horizontally (Trung 2021; Trung and Tuan 2014; Ai et al. 2020). Figure 1b shows the Rx lens accumulates the transmitted optical beam (Tx), which is projected onto the receiver (Rx) plane's surface. The incoming optical signal then converges

onto the surface of the APD's area (Trung 2021). Addition to the optical signal, the thermal noise, and the background noise is also added to the receiver (Trung 2021).

The expression for θ_a in the horizontal flying state is $\theta_a = \theta - \varphi$. The link will thus be interrupted when it crosses the receiver's field of view (FOV). The PDF of θ_a is given by Zheng et al. (2021); Dabiri et al. 2019):

$$f(\theta_a) = \frac{|\theta - \varphi|}{\sigma_{r_0}^2 + \sigma_{t_0}^2} \exp\left(-\frac{(\theta - \varphi)^2}{2\left(\sigma_{r_0}^2 + \sigma_{t_0}^2\right)}\right) \tag{7}$$

where $\sigma_{t_0}^2$ and $\sigma_{r_0}^2$ are the variances of the angle deviation of the transmitter and the receiver, respectively. θ can be expressed as (Zheng et al. 2021):

$$\theta = \sqrt{\left(\theta_{tx} + \theta_{rx}\right)^2 + \left(\theta_{ty} + \theta_{ry}\right)^2} \tag{8}$$

where θ_{tx} and θ_{rx} represent the x-direction angle deviations of the transmitting and receiving ends, respectively, and θ_{ty} and θ_{ry} represent the y-direction angle deviations of the transmitting and receiving ends, respectively. The PDF of θ_t can be written as (Zheng et al. 2021; Dabiri et al. 2019):

$$f(\theta_t) = \frac{\theta_t}{\sigma_{t_0}^2} \exp\left(-\frac{\theta_t^2}{2\sigma_{t_0}^2}\right) \tag{9}$$

$$r_d = r_{d_r} + r_{d_t} + Z\hat{\theta}_t \tag{10}$$

where $r_{d_r} = x_r + y_r$ is the receiving end's position deviation, $r_{d_t} = x_t + y_t$ is the transmitting end's position deviation, Z is the z-plane transmission distance, and $\hat{\theta}_t = \hat{\theta}_{tx} + \hat{\theta}_{ty}$ is the transmitting end's angle deviation. r_d conditioned on Rician distribution for $\hat{\theta}_{tx}$ and $\hat{\theta}_{ty}$. Therefore, the geometric and PE coefficients can be expressed as (Zheng et al. 2021; Trung 2021; Trung and Tuan 2014; Ai et al. 2020):

$$\begin{aligned} h_g &= \int\int_A \frac{2}{\pi\omega_z^2} \exp\left[-2\frac{(r + r_d)^2}{\omega_z^2}\right] ds \\ &= \int_{-a}^{a} \int_{-\sqrt{\frac{a^2-y^2}{\zeta^2}}}^{\sqrt{\frac{a^2-y^2}{\zeta^2}}} \frac{2}{\pi\omega_z^2} \exp\left[-2\frac{\left(x + x_r + x_t + Z\theta_{tx}\right)^2 + \left(y + y_r + y_t + Z\theta_{ty}\right)^2}{\omega_z^2}\right] dydx \end{aligned} \tag{11}$$

$$h_g \approx \frac{1}{\zeta^2} A_0 \exp\left(\frac{-2r_d^2}{\omega_{zeq}^2}\right) \tag{12}$$

where $A_0 = \left[erfc(v)\right]^2$ represents the lens's energy-to-total energy ratio when $r_d = 0$. Using the avalanche photodiode (APD) or PIN photodetectors (PDs), the Rx lens collects the

received beam onto the PD area. The equivalent beam waist can be calculated as (Zheng et al. 2021; Trung 2021; Trung and Tuan 2014; Ai et al. 2020)

$$\omega_{zeq}^2 = \omega_z^2 \frac{\sqrt{\pi}\,\mathrm{erfc}(\upsilon)}{2\upsilon \exp\left(-\upsilon^2\right)} \tag{13}$$

where erfc (·) is the error function and $\upsilon = \sqrt{\pi}a/\sqrt{2}\omega_z$. $\zeta = 1/cos\alpha$, ω_z is the beam waist of distance Z, and a is the Rx lens radius. The PDF of h conditioned on θ_t can be expressed as (Zheng et al. 2021). $r_{d_r} \sim N\left(0, \sigma_{r_p}^2\right)$, $r_{d_t} \sim N\left(0, \sigma_{t_p}^2\right)$, $\theta_t \sim N\left(0, \sigma_{t_0}^2\right)$, and $\alpha \sim N\left(0, \sigma_\alpha^2\right)$ respectively (Zheng et al. 2021; Dabiri et al. 2019), where $\sigma_{t_p}^2$ and $\sigma_{r_p}^2$ are the variances of the UAV's position deviation at the transmitting and receiving ends. $\sigma_{t_0}^2$ is the variance of the UAV's aiming angle deviation at the transmitting end and σ_α^2 is the variance of the UAV's jitter angle at the receiving end (Zheng et al. 2021; Trung 2021; Trung and Tuan 2014; Ai et al. 2020)

$$f\left(h|\theta_t\right) = \left\{1 - \left[\frac{1}{2}\exp\left(-\frac{\left(\theta_{FOV} - \varphi\right)^2}{2\left(\sigma_{r_0}^2 + \sigma_{t_0}^2\right)}\right) + \frac{1}{2}\exp\left(-\frac{\left(\theta_{FOV} + \varphi\right)^2}{2\left(\sigma_{r_0}^2 + \sigma_{t_0}^2\right)}\right)\right]\right\} \times \int_0^\infty \frac{1}{h_t} f_{h_t}\left(h_t\right)\, dht \tag{14}$$

where θ_{FOV} is the Rx's field-of-view (FOV) angle (Zheng et al. 2021; Trung 2021; Trung and Tuan 2014; Ai et al. 2020). Then the PDF of h can be given as:

$$f(h) = \int_0^\infty f\left(h|\theta_t\right) f\left(\theta_t\right) d\theta_t \tag{15}$$

3 Symbol error rate calculation

The outage probability (OP) of the UAV-FSO communication can be expressed as (Zheng et al. 2021; Trung 2021; Trung and Tuan 2014; Ai et al. 2020; El-Mottaleb et al. 2021; El-Fikky et al. 2020):

$$P_{out} = \int_0^{h_{th}} f(h)dh \tag{16}$$

where h_{th} is the channel coefficient threshold of h. The link outage can be taken into consideration when the instantaneous channel coefficient is lower than h_{th}. Equation (17) can be used to calculate the average BER when taking into account the quadrature phase shift keying (QPSK) modulation scheme (Zheng et al. 2021; Dabiri et al. 2019; Trung 2021; Trung and Tuan 2014; Ai et al. 2020; El-Mottaleb et al. 2021; El-Fikky et al. 2020):

$$P_e = \frac{1}{2}\int_0^\infty \mathrm{erfc}\left(\sqrt{\frac{\gamma h}{2}}\right) f(h)dh \tag{17}$$

where g is the transmitter's signal-to-noise ratio (SNR) and the complementary error function is erfc (). In order to account for the aiming inaccuracy and fluctuations from the FSO Tx installed on the UAV to the FSO Rx, we calculate the SER in the weak turbulence (WT), moderate turbulence (MT), and strong turbulence (ST) channels. The generalized average SER expression for assessing the UAV-based FSO system considering the LN and GG fading channels is given by Trung (2021); Trung and Tuan 2014; Ai et al. 2020; El-Mottaleb et al. 2021; El-Fikky et al. 2020).

$$\mathrm{SER} = \int_0^\infty \mathrm{P_e(h) f_h(h) dh}, \tag{18}$$

where $P_e(h)$ represents the conditional error probability (CEP) and $f_h(h)$ is the PDF of SNR, h. By employing a general $(M_I \times M_Q)$-quadrature amplitude modulation (QAM) constellation with two independents M_I in-phase and M_Q quadrature signal amplitudes, the CEP is given by Trung (2021); Trung and Tuan 2014; Ai et al. 2020)where $f_h(h)$ is the PDF of SNR, h. $P_e(h)$ denotes the CEP. Using a general $(M_I \times M_Q)$-QAM constellation with two independents M_I in-phase and M_Q quadrature signal amplitudes, the CEP is given by Trung (2021); Trung and Tuan 2014; Ai et al. 2020)

$$\begin{aligned} \mathrm{P_e(h)} = {} & 2\mathrm{q(M_I)Q}\left(\mathrm{A_I}\sqrt{\mathrm{h}}\right) + 2\mathrm{q(M_Q)Q}\left(\mathrm{A_Q}\sqrt{\mathrm{h}}\right) \\ & - 4\mathrm{q(M_I)q(M_Q)Q}\left(\mathrm{A_I}\sqrt{\mathrm{h}}\right)\mathrm{Q}\left(\mathrm{A_Q}\sqrt{\mathrm{h}}\right) \end{aligned} \tag{19}$$

where $q(\mathrm{x}) = 1 - \mathrm{x}^{-1}$, the Gaussian Q-function is defined by Trung (2021); Trung and Tuan 2014; Ai et al. 2020)

$$Q(\mathrm{x}) = 0.5\ \mathrm{erfc}\left(\mathrm{x}/\sqrt{2}\right) = 1/\sqrt{2\pi}\int_{\mathrm{x}}^{\infty} \exp\left(-\mathrm{t}^2/2\right)\mathrm{dt} \tag{20}$$

where $Q(x)$ refers to the complementary error function. M_I, M_Q can be used to compute the in-phase and quadrature distances A_I and A_Q (Trung 2021; Trung and Tuan 2014; Ai et al. 2020).

$$\mathrm{A_I} = \left[6/\left(\mathrm{M_I^2} - 1\right) + \mathrm{d_{IQ}^2}\left(\mathrm{M_Q^2} - 1\right)\right]^{\frac{1}{2}} \tag{21}$$

$$\mathrm{A_Q} = \left[6\mathrm{d_{IQ}^2}/\left(\mathrm{M_I^2} - 1\right) + d_{\mathrm{IQ}}^2\left(\mathrm{M_Q^2} - 1\right)\right]^{\frac{1}{2}} \tag{22}$$

where $d_{IQ} = \frac{d_Q}{d_I}$. The SER is then calculated by

$$\begin{aligned} \mathrm{SER} = {} & 2\mathrm{q(M_I)}\int_0^\infty \mathrm{Q}\left(\mathrm{A_I}\sqrt{\mathrm{h}}\right)\mathrm{f_h(h)dh} + 2\mathrm{q(M_Q)}\int_0^\infty \mathrm{Q}\left(\mathrm{A_Q}\sqrt{\mathrm{h}}\right)\mathrm{f_h(h)dh} \\ & - 4\mathrm{q(M_I)q(M_Q)}\int_0^\infty \mathrm{Q}\left(\mathrm{A_I}\sqrt{\mathrm{h}}\right)\mathrm{Q}\left(\mathrm{A_Q}\sqrt{\mathrm{h}}\right)\mathrm{f_h(h)dh}. \end{aligned} \tag{23}$$

3.1 SER calculation of WT to MT turbulence

The PDF of LN channels can be expressed for WT to MT turbulence (Zheng et al. 2021; Yousif and Elsayed 2019; Trung 2021; Trung and Tuan 2014; Ai et al. 2020)

$$f_{\mathrm{f_h}}^{\mathrm{LN}}(\mathrm{h}) = \exp\left(-\frac{\theta_{\mathrm{FOV}}^2}{2\sigma_{\mathrm{r_0}}^2 \mathrm{A}_0}\right)\delta\left(\frac{\sigma_n\sqrt{h}}{P_t mGR}\right) + \mathrm{E}_{\S 1}\left[1-\exp\left(-\frac{\theta_{\mathrm{FOV}}^2}{2\sigma_{\mathrm{r_0}}^2 \mathrm{A}_0}\right)\right] X^{\mathrm{E}_{\S 2}} Q\left(\frac{\ln\left(\frac{\frac{\sigma_n\sqrt{h}}{P_t mGR}}{A_0\exp\left(-\mathrm{h}l_{fso}\right)}\right)+\mathrm{E}_{\S 3}}{\sigma_R}\right) \tag{24}$$

$$X^2 = \frac{h\sigma_n^2}{P_t^2 m^2 G^2 R^2} \rightarrow X = \frac{\sigma_n\sqrt{h}}{P_t mGR}. \tag{25}$$

where R and G denote the APD responsivity and the average gain, respectively. σ_n is the thermal variance, m, and P_t are the modulation index and average transmitted power per symbol, respectively. $\mathrm{E}_{\S 1} = \frac{\Psi}{(A_0 h_t)^{\Psi}}\exp\left[0.5\sigma_{\mathrm{R}}^2\Psi(1+\Psi)\right], \mathrm{E}_{\S 2} = \Psi - 1, \mathrm{E}_{\S 3} = 0.5\sigma_{\mathrm{R}}^2\Psi(1+2\Psi)$. $Q(\cdot)$ is the Q - function and $\Psi = \frac{\omega_{zeq}^2}{4\left(\mathrm{l}_{\mathrm{fso}}^2\sigma_{\mathrm{t_0}}^2+\sigma_{\mathrm{r_p}}^2+\sigma_{\mathrm{t_p}}^2\right)}\Psi = \frac{\omega_{\mathrm{zeq}}^2}{4\left(\mathrm{l}_{\mathrm{fso}}^2\sigma_{\mathrm{t_0}}^2+\sigma_{\mathrm{r_p}}^2+\sigma_{\mathrm{t_p}}^2\right)}$.

$$\begin{aligned}
SER^{LN} = {} & 2\mathrm{q}(\mathrm{M}_I)\int_0^{\infty}\left(Q\left(A_I\sqrt{h}\right)\exp\left(\frac{\theta_{\mathrm{FOV}}^2}{2\sigma_{\mathrm{r_0}}^2 \mathrm{A}_0}\right)\delta\left(\frac{\sigma_n\sqrt{h}}{P_t mGR}\right)\right. \\
& \left. + \mathrm{E}_{\S 1}\left(\left[1-\exp\left(\frac{\theta_{\mathrm{FOV}}^2}{2\sigma_{\mathrm{r_0}}^2 A_0}\right)\right] X^{\mathrm{E}_{\S 2}} Q\left(\frac{\ln\left(\frac{\frac{\sigma_n\sqrt{h}}{P_t mGR}}{A_0\exp\left(-\mathrm{h}l_{fso}\right)}\right)+\mathrm{E}_{\S 3}}{\sigma_R}\right)\right)\right) dh \\
& + 2q\left(\mathrm{M_Q}\right)\int_0^{\infty}\mathrm{Q}\left(\mathrm{A_Q}\sqrt{\mathrm{h}}\right)exp\left(-\frac{\theta_{\mathrm{FOV}}^2}{2\sigma_{\mathrm{r_0}}^2 A_0}\right)\delta\left(\frac{\sigma_n\sqrt{h}}{P_t mGR}\right) \\
& + \left(\mathrm{E}_{\S 1}\left[1-\exp\left(-\frac{\theta_{\mathrm{FOV}}^2}{2\sigma_{\mathrm{r_0}}^2 A_0}\right)\right] X^{\mathrm{E}_{\S 2}} Q\left(\frac{\ln\left(\frac{\frac{\sigma_n\sqrt{h}}{P_t mGR}}{A_0\exp\left(-\mathrm{h}l_{fso}\right)}\right)+\mathrm{E}_{\S 3}}{\sigma_R}\right)\right) dh \\
& - 4\mathrm{q}(\mathrm{M_I})\mathrm{q}(\mathrm{M_Q})\int_0^{\infty}\mathrm{Q}\left(\mathrm{A_I}\sqrt{\mathrm{h}}\right)\mathrm{Q}\left(\mathrm{A_Q}\sqrt{\mathrm{h}}\right)\exp\left(\frac{\theta_{\mathrm{FOV}}^2}{2\sigma_{\mathrm{r_0}}^2 A_0}\right)\delta\left(\frac{\sigma_n\sqrt{h}}{P_t mGR}\right) \\
& + \mathrm{E}_{\S 1}\left(\left[1-\exp\left(-\frac{\theta_{\mathrm{FOV}}^2}{2\sigma_{\mathrm{r_0}}^2 A_0}\right)\right] X^{\mathrm{E}_{\S 2}} Q\left(\frac{\ln\left(\frac{\frac{\sigma_n\sqrt{h}}{P_t mGR}}{A_0\exp\left(-\mathrm{h}l_{fso}\right)}\right)+\mathrm{E}_{\S 3}}{\sigma_R}\right)\right) \mathrm{dh}.
\end{aligned} \tag{26}$$

3.2 SER calculation of MT to ST turbulence

From Eqs. (14), (24), and (25), the PDFs and SER of the MT to ST turbulence regimes can be derived as (Zheng et al. 2021; Yousif and Elsayed 2019; Elsayed and Yousif 2020; Elsayed et al. 2018; Dabiri et al. 2019; Trung 2021; Trung and Tuan 2014; Ai et al. 2020)

$$f_{\mathrm{f_h}}^{GG}(h) = \exp\left(-\frac{\theta_{\mathrm{FOV}}^2}{2\sigma_{\mathrm{r_0}}^2 A_0}\right)\delta\left(\frac{\sigma_n\sqrt{h}}{P_t mGR}\right) + \mathrm{E_{\S}}_1\left[1 - exp\left(-\frac{\theta_{\mathrm{FOV}}^2}{2\sigma_{\mathrm{r_0}}^2 A_0}\right)\right] \sum_{n=0}^{N}\left(c_1\left(\frac{\sigma_n\sqrt{h}}{P_t mGR}\right)^{\Psi-1} + c_2\left(\frac{\sigma_n\sqrt{h}}{P_t mGR}\right)^{n+\alpha-1} - c_3\left(\frac{\sigma_n\sqrt{h}}{P_t mGR}\right)^{n+\beta-1}\right) \tag{27}$$

The closed-form expressions for SER of the UAV-based FSO communication links of MT to ST conditions can be calculated as (Zheng et al. 2021; Yousif and Elsayed 2019; Elsayed and Yousif 2020; Elsayed et al. 2018; Dabiri et al. 2019; Trung 2021; Trung and Tuan 2014; Ai et al. 2020)

$$\begin{aligned}
SER^{GG} = {} & 2\mathrm{q}(\mathrm{M_I})\int_0^{\infty}\left(Q\left(A_I\sqrt{h}\right)exp\left(-\frac{\theta_{\mathrm{FOV}}^2}{2\sigma_{\mathrm{r_0}}^2 A_0^2}\right)\delta\left(\frac{\sigma_n\sqrt{h}}{P_t mGR}\right)\right. \\
& + \mathrm{E_{\S}}_1\left[1 - exp\left(-\frac{\theta_{\mathrm{FOV}}^2}{2\sigma_{\mathrm{r_0}}^2 A_0}\right)\right]\sum_{n=0}^{N}\left(c_1\left(\frac{\sigma_n\sqrt{h}}{P_t mGR}\right)^{\Psi-1} + c_2\left(\frac{\sigma_n\sqrt{h}}{P_t mGR}\right)^{n+\alpha-1}\right. \\
& \left.\left. - c_3\left(\frac{\sigma_n\sqrt{h}}{P_t mGR}\right)^{n+\beta-1}dh\right)\right) \\
& + 2q(\mathrm{M_Q})\int_0^{\infty}\mathrm{Q}\left(\mathrm{A_Q}\sqrt{\mathrm{h}}\right)exp\left(-\frac{\theta_{\mathrm{FOV}}^2}{2\sigma_{\mathrm{r_0}}^2 A_0}\right)\delta\left(\frac{\sigma_n\sqrt{h}}{P_t mGR}\right) \\
& + \left(\mathrm{E_{\S}}_1\left[1 - exp\left(-\frac{\theta_{\mathrm{FOV}}^2}{2\sigma_{\mathrm{r_0}}^2 A_0}\right)\right]\right)\sum_{n=0}^{N}\left(c_1\left(\frac{\sigma_n\sqrt{h}}{P_t mGR}\right)^{\Psi-1} + c_2\left(\frac{\sigma_n\sqrt{h}}{P_t mGR}\right)^{n+\alpha-1}\right. \\
& \left. - c_3\left(\frac{\sigma_n\sqrt{h}}{P_t mGR}\right)^{n+\beta-1}\right)dh \\
& - 4\mathrm{q}(\mathrm{M_I})\mathrm{q}(\mathrm{M_Q})\int_0^{\infty}\mathrm{Q}\left(\mathrm{A_I}\sqrt{\mathrm{h}}\right)\mathrm{Q}\left(\mathrm{A_Q}\sqrt{\mathrm{h}}\right)exp\left(-\frac{\theta_{\mathrm{FOV}}^2}{2\sigma_{\mathrm{r_0}}^2 A_0}\right)\delta\left(\frac{\sigma_n\sqrt{h}}{P_t mGR}\right) \\
& + \left(\mathrm{E_{\S}}_1\left[1 - exp\left(-\frac{\theta_{\mathrm{FOV}}^2}{2\sigma_{\mathrm{r_0}}^2 A_0}\right)\right]\right)\sum_{n=0}^{N}\left(c_1\left(\frac{\sigma_n\sqrt{h}}{P_t mGR}\right)^{\Psi-1} + c_2\left(\frac{\sigma_n\sqrt{h}}{P_t mGR}\right)^{n+\alpha-1} - c_3\left(\frac{\sigma_n\sqrt{h}}{P_t mGR}\right)^{n+\beta-1}\right)dh.
\end{aligned} \tag{28}$$

In Eq. (28), $C_1 = \left(C_4C_5X_m^{n+\beta-\Psi} - C_4C_6X_m^{n+\alpha-\Psi}\right)$, $C_2 = \frac{C_4C_6}{\left(h_tA_0\right)^{n+\alpha-\Psi}}$, $C_3 = \frac{C_4C_5}{\left(h_tA_0\right)^{n+\beta-\Psi}}$, $C_4 = \frac{\pi\mathrm{E_{\S}}}{\left(h_tA_0\right)\mathrm{E_{\S}}\Gamma(\alpha)\Gamma(\beta)\sin(\pi(\alpha-\beta))}$, $C_5 = \frac{\alpha\beta^{(n+\beta)}}{\left(n+\beta-\mathrm{E_{\S}}\right)\Gamma(n-\alpha+\beta+1)n!}$ and $C_6 = \frac{\alpha\beta^{(n+\alpha)}}{\left(n+\beta-\mathrm{E_{\S}}\right)\Gamma(n+\alpha-\beta+1)n!}$ (Zheng et al. 2021; Yousif and Elsayed 2019; Dabiri et al. 2019; Trung 2021; Trung and Tuan 2014; Ai et al. 2020). N is a natural number and $\mathrm{X_m}$ is a coefficient depends on the Rytov variance σ_{R}^2 (Zheng et al. 2021; Yousif et al. 2019; Yousif and Elsayed 2019; Dabiri et al. 2019; Trung 2021; Trung and Tuan 2014; Ai et al. 2020).

$$\sigma_n^2 = \sigma_{bg}^2 + \sigma_{th}^2 + \sigma_s^2, \tag{29}$$

where $\sigma_{bg}^2, \sigma_{th}^2$, and σ_s^2 are the noise variances due to background noise, thermal noise, and shot noise, respectively (Zheng et al. 2021; Yousif and Elsayed 2019; Dabiri et al. 2019; Trung 2021; Trung and Tuan 2014; Ai et al. 2020).

$$\sigma_s^2 = 2eGFB_e\eta P_t. \tag{30}$$

In Eq. (30), F denotes excess noise factor of APD, $\eta = \frac{eGR}{h_{planck}v}$, where h_{planck} is the Planck constant, optical frequency $v = c/\lambda$, e and c denote the electron charge (coulombs) and the speed of light in a vacuum (m/s), respectively (Zheng et al. 2021; Yousif et al. 2019; Yousif and Elsayed 2019; Trung 2021; Trung and Tuan 2014; Ai et al. 2020).

$$\sigma_{th}^2 = \frac{4k_BTB_e}{R_L}, \tag{31}$$

where R_L, T, and k_B are APD's load resistance, Rx's temperature in degrees Kelvin, and Boltzmann constant, respectively (Zheng et al. 2021; Yousif et al. 2019; Yousif and Elsayed 2019; Trung 2021; Trung and Tuan 2014; Ai et al. 2020)

4 Numerical results and discussion

In this section, the FSO communication link is simulated when the receiving UAV is in straight-flight mode. The UAV-FSO relay-assisted system parameters utilized in the calculations are shown in Table 1. The proposed model is implemented under the MATLAB software platform. The Monte Carlo simulation is used to model the probability of different results and the accuracy of the simulated data. By considering the angle pointing deviation and position deviation produced by the UAV jitter, the effect of the UAV's fuselage tilt angle in horizontal and straight flights on the communication quality is examined. The following initial settings have been made: a wavelength of 1550 nm, a beam waist of 5 mm, a radius of 0.1 m for the receiver aperture, and a maximum UAV-FSO transmission range of $L_{fso} = 2$ km. The power spectral density function is simulated using the Modified Von Karman model, where the transmission rate of the QSPK signal is 20 Gb/s and ARIS $C_n^2 = 1 \times 10^{-13} m^{-2/3}$ for ST, $5 \times 10^{-15} m^{-2/3}$ for MT, and $1 \times 10^{-17} m^{-2/3}$ for WT. The values of $\sigma_{r_0}^2 = \sigma_{t_0}^2 = 1$ mrad and the tilt angles of the fuselage φ as 0, 5, 10, 20, and 25 mrad, respectively, were used in the simulation. As observed in Fig. 2, the tilt angle of the fuselage has a greater impact on the communication quality of UAVs than does the jitter induced by the wind resistance. In Fig. 2, the OP increases the UAVs-FSO communication with the increase of the random wind resistance and the PE with AT. The OP increases to 10^{-4} at a SNR of 25 dB when σ_α^2 increases from 0 to 7 mrad. When σ_α^2 increases from 0 to 7 mrad at the OP of 10^{-4}, the SNR should be increased from 17 dB to more than 25 dB. The required SNR is $\geq$25 dB when the variance of the wind σ_α^2 is 1 mrad at an OP of 10^{-6}. In Fig. 3, the average BER (ABER) will also increase when σ_α^2 increases. The ABER will increase from 10^{-7} to 3.38×10^{-5} at the SNR of 23 dB, when σ_α^2 increases from 0 to 7 mrad. With the ABER of 10^{-6}, the SNR should be 16.23 dB, 17.64 dB, and 21.45 dB when σ_α^2 is 0 mrad, 1 mrad, and 2 mrad, respectively. With the ABER is 10^{-5} and σ_α^2 is 5 mrad, the

Table 1 UAV-FSO system parameters used in the calculations

Parameter	Description	Value setting
λ	Signal center wavelength	1550 nm
ω_z	Beam waist	5 mm
r_d	Receiver aperture radius	0.1 m
σ_α^2	The variance of the jitter angle of the UAV at the receiver	0, 1 mrad, 2 mrad, 5 mrad, and 7 mrad
φ	Tilt angles of the fuselage	0, 5 mrad, 10 mrad, 20 mrad, and 25 mrad
L_{fso}	Maximum hovering UAV-FSO link length	2 km
θ_{FOV}	Receiver's field angle	40 mrad
C_n^2	Strength of weak turbulence (WT)	$1 \times 10^{-17} m^{-2/3}$
C_n^2	Strength of moderate turbulence (MT)	$5 \times 10^{-15} m^{-2/3}$
C_n^2	Strength of strong turbulence (ST)	$1 \times 10^{-13} m^{-2/3}$
$\sigma_{t_0}^2$	The variance of the pointing angle deviation of the UAV at the transmitter	1 mrad
$\sigma_{r_0}^2$	The variance of the pointing angle deviation of the UAV at the receiver	1 mrad
h_g	Geometric and pointing error coefficient deviation	0.05 mrad
$\sigma_{t_p}^2$	The variance of the position deviation of the UAV at the transmitter	6 cm
$\sigma_{r_p}^2$	The variance of the position deviation of the UAV at the receiver	6 cm
θ_{tx}	Angle deviation of the transmitter in the *x* direction	1 mrad
M_I, M_Q	In-phase, quadrature distances	8, 4
G	Average APD gain	18 dB, 30 dB
m	Modulation index	1
P_t	Average transmitted power per symbol	− 15 dBm, 5 dBm
R	Responsivity	0.6 A/W
X	Attenuation coefficient	3.436
h_t	Attenuation coefficient (very clear air)	0.0647 dB/km
h_t	Attenuation coefficient (clear air)	0.2208 dB/km
h_t	Attenuation coefficient (haze)	0.7360 dB/km

Table 1 (continued)

Parameter	Description	Value setting
B_e	Electrical bandwidth	10^9 Hz
h_{planck}	The Planck constant	6.626×10^{-34} m$^2 \cdot$ Kg/s
R_L	APD's load resistance	1000 Ω
T	Receiver noise temperature	300° K
k_B	Boltzmann's constant	1.38×10^{-23} J/K
e	Electron charge	$1.602176634 \times 10^{-19}$ coulombs
F	Excess noise factor of APD	2.75
c	The speed of light in a vacuum	299,792,458 m/s

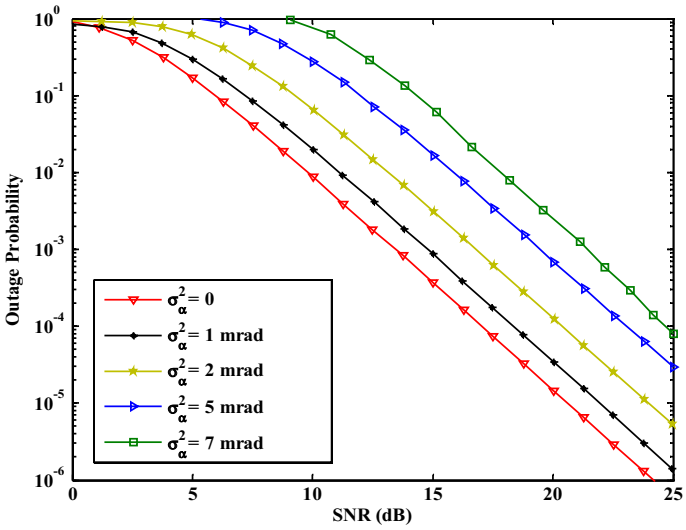

Fig. 2 OP versus SNR (dB) in UAV-FSO communication link with the different wind resistance σ_α^2 with at $l_{fso} = 2$ km

SNR reaches 18.77 dB while when σ_α^2 is 7 mrad, the ABER is 10^{-4} and the SNR is 10.05 dB.

The UAV-based FSO system performance is shown in Fig. 4 about the average SNR for 8-PSK and 16-QAM, with/without PE. The simulation was performed to verify the analytical expressions. The system included WT to MT atmospheric turbulence conditions from $C_n^2 = 1 \times 10^{-17} m^{-2/3}$ to $5 \times 10^{-15} m^{-2/3}$. The geometric/PE coefficient deviation $h_g = 0.05$

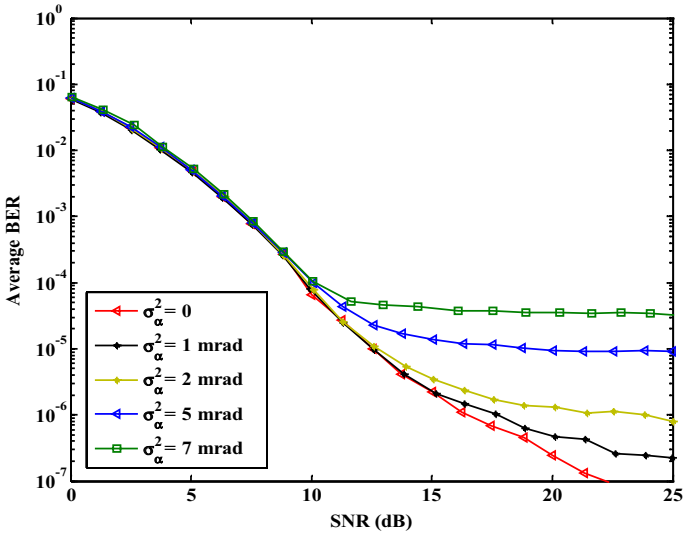

Fig. 3 ABER versus SNR (dB) in UAV-FSO communication link with the different σ_α^2 with at $l_{fso} = 2$ km

and the FSO link distance L = 1000 m. As can be observed, the SER with PE is much worse than when there isn't PE. On the other hand, using a high-order modulation method causes the SER to be less than desired. Using 8-PSK modulation without PE requires 23.5 dB at BER of 10^{-8} while 16-QAM without PE requires 26.5 dB to maintain the same BER of 10^{-8}. Compared with 16-QAM without PEs, the signal-to-noise ratio (SNR) gain of 8-PSK without PE is 3 dB. The SNR power penalty is 3 dB at BER of 10^{-8}.

When the BER is 10^{-4}, the 8-PSK with PE needs 22.69 dB at BER while the 16-QAM with PE needs 26.28 to maintain the same BER. The SNR power penalty is 3.59 dB. When BER is 10^{-4}, compared to the 16-QAM scheme with a PE, the SNR gain of the 8-PSK scheme with a PE is 3.59 dB. At the target BER = 10^{-3}, the 8-PSK without PE requires 13.50 dB while the 16-QAM scheme without PE requires 15.50 dB. So, the 8-PSK scheme without PE can achieve a 2 dB power gain compared with the 16-QAM scheme without PE. At the target BER = 10^{-3}, the 8-PSK with PE requires 20.37 dB while the 16-QAM scheme with PE requires 24.12 dB. So, the 8-PSK scheme with PE can be achieved a 3.75 dB power gain compared with the 16-QAM scheme with PE.

Figure 5 shows the SER versus APD gain for various ARIS C_n^2 in the WT, MT, and ST at L of 1000 m. In the WT at $C_n^2 = 1 \times 10^{-17} m^{-2/3}$, the SER performance improves and reaches to 10^{-11} while in the MT, the SER is at 10^{-6} and in the ST, the SER decreases to 10^{-5}. Therefore, the turbulence strength influences how well the SER performs. When the atmospheric turbulence increases, the SER decrease. It is observed that weather-related turbulence conditions significantly impact SER performance (El-Mottaleb et al. 2021; El-Fikky et al. 2020). Additionally, as the APD's gain is raised, the noise variances are caused by the desired received signal of σ_α^2 rise as well.

Figure 6 shows the OP versus SNR for a traditional relay-assisted system with four stationary relays. The simulation results confirm the enormous potential of buffer-aided relays to improve OP performance, particularly in both medium and high SNR regimes (Fawaz

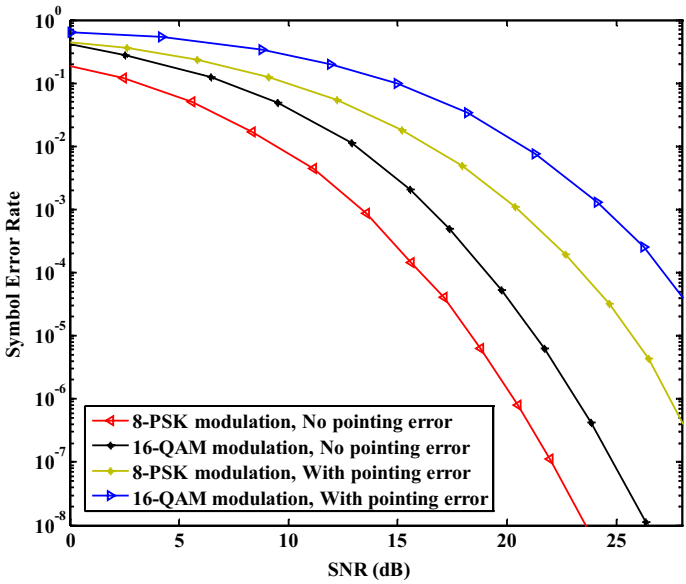

Fig. 4 SER versus SNR for M-PSK and M-QAM schemes with/without pointing errors

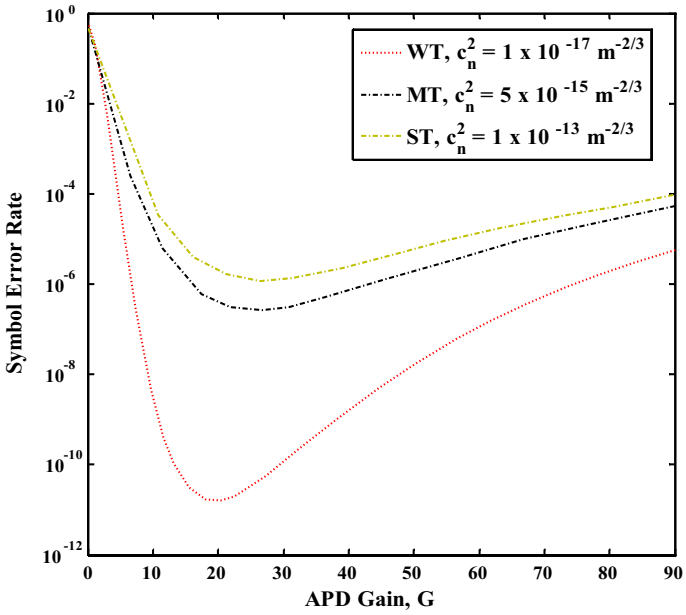

Fig. 5 SER versus APD gain, for different values of C_n^2 at a FSO link distance $l_{fso} = 1$ km

et al. 2018). For instance, with an SNR of 20 dB, an OP of around 10^{-7} is seen compared to 10^{-1} for the conventional system. Since a good channel quality would enable the transmission of several packets from the UAVs' buffers to the target. As a result, this enhances the OP of the FSO system (Fawaz et al. 2018). Figure 6 shows the performance of the UAV-FSO system compared with a conventional FSO (CFSO) system. The OP in the CFSO of 10^{-1} while using a UAV-FSO system with four relays, the OP can reach 10^{-7}. Using relay UAV-FSO, we achieve high SNR at 20 dB at the OP of 10^{-7}. The UAV-FSO system with a UAV altitude of 250 m can reach 3.7×10^{-7} while with a UAV altitude of 500 m, achieve OP of 10^{-6}. When the UAV altitude increase, the OP increase. The UAV-FSO system performance with four stationary relays can achieve better OP and SNR. The results show the relay-assisted.

UAV-FSO system with four stationary relays can achieve better BER performance of 10^{-6} at 20 dB SNR, while the CFSO can achieve BER of 10^{-1} at 20 dB SNR. The BER of a CFSO relay-assisted FSO system and a UAV-FSO system with five stationary relays are compared in Fig. 7. In terms of packet delivery, the results demonstrate that a moving buffer-aided relay performs better than a stationary buffer-free relay. The results show a steady improvement over the CFSO system in terms of OP. It can be seen that AT and PEs affect the BER with different severity. For example, heavy weather turbulence degrades the SNR and raises the BER (El-Mottaleb et al. 2021; El-Fikky et al. 2020). As far as AT and PEs are concerned, they affect BER equally. Here, the SNR increases in the ideal situation without AT but falls with an increase in PE and AT. The BER performance is also enhanced. The results show the relay-assisted UAV-FSO system with five stationary relays can achieve BER 10^{-8} at 25 dB SNR in the ideal case and 10^{-5} at 27 dB SNR with AT and PE at an FSO length 1000 m. The results show the relay UAV-FSO system outperforms the CFSO at the BER and SNR performance.

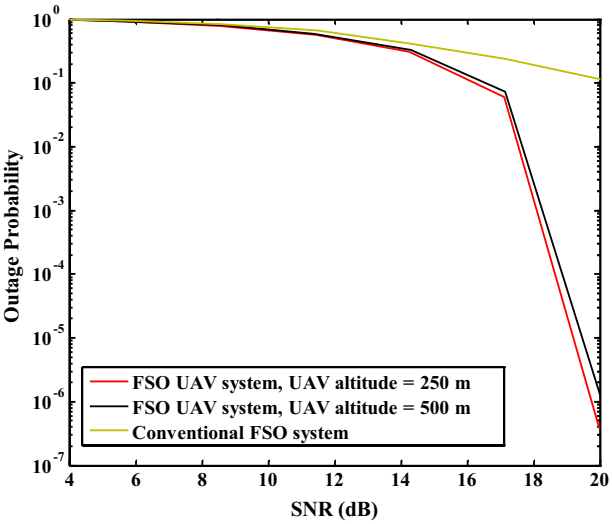

Fig. 6 OP versus SNR (dB) of UAV with 4 stationary relays-assisted and buffer-aided relay UAV-FSO systems

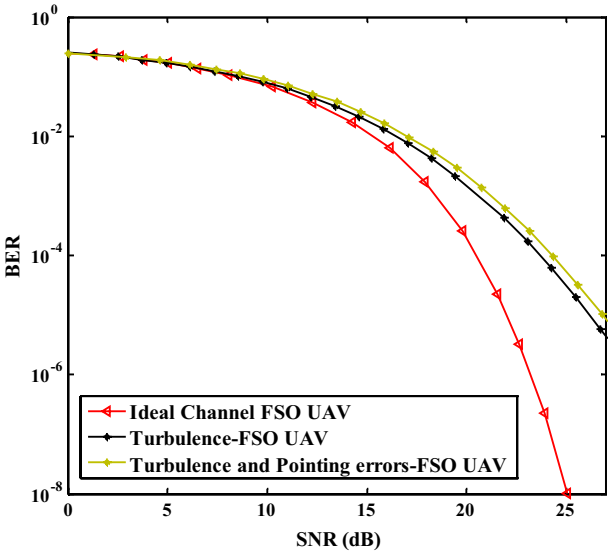

Fig. 7 BER versus SNR (dB) of UAV with 5 stationary relays and buffer-aided relay-assisted UAV-FSO system at an FSO link distance $l_{fso} = 1$ km

Figure 8 shows the symbol error rate (SER) versus UAV-FSO link length, L_{fso} for different values of C_n^2 of the geometric and pointing error coefficient deviation $h_g = 0.05$ mrad. The effects of UAV'FSO s fluctuation increase when the UAV-FSO link length, L_{fso} increases. As we can observe, the results of the weak turbulence achieve better SER

compared with MT and ST. The obtained results show that decreasing L_{fso} can compensate for the effects of UAV-FSO link fluctuation on the proposed system (Trung 2021). Figure 9 shows the comparison between the atmospheric turbulence transmission with pointing error (PE) and without PE for BER versus the average transmitted power per symbol P_t, for different turbulence strengths C_n^2 ($m^{-2/3}$) at $L_{fso} = 2$ km. The numerical results show that the required P_t to obtain BER of 10^{-9} are -12.7 dBm, -10.8 dBm, and -10 dBm corresponding to $C_n^2 = 1 \times 10^{-17} m^{-2/3}$, $C_n^2 = 5 \times 10^{-15} m^{-2/3}$, and $C_n^2 = 1 \times 10^{-13} m^{-2/3}$ for hovering UAV-FSO without PE, respectively (Elsayed et al. 2018). Without PE, the BER performance is significantly improved compared to in the presence of PE. The required P_t to obtain BER of 10^{-9} are -9.2 dBm, -8 dBm, and -6.8 dBm corresponding to $C_n^2 = 1 \times 10^{-17} m^{-2/3}$, $C_n^2 = 5 \times 10^{-15} m^{-2/3}$, and $C_n^2 = 1 \times 10^{-13} m^{-2/3}$ for hovering UAV-FSO with PE, respectively. The performance improvements without PE are 3.5 dB, 2.8 dB, and 3.2 dB for $C_n^2 = 1 \times 10^{-17} m^{-2/3}$, $C_n^2 = 5 \times 10^{-15} m^{-2/3}$, and $C_n^2 = 1 \times 10^{-13} m^{-2/3}$, respectively.

5 Conclusion

In this paper, a new FSO communication channel model for the hovering UAV-FSO OWC fluctuations under the PEs, AT effects, jitter, deviation, receiving an error, and wind resistance effects is established. To improve the performance of hovering UAV-based FSO relay OWC systems. We reduce the influence of UAV-FSO OWC fluctuations under PEs and AT effects. By receiving incoherent signals at various locations, the spatial diversity-based relay-assisted NFSO systems can significantly increase the system's redundancy and enhance connection stability. A UAV-FSO communication channel model has been investigated using different performance metrics. Along with the air turbulence and the jitter, the UAV suffers due to its engine vibration; the tilt angle and the horizontal lateral wind resistance generated by the UAV's various motion

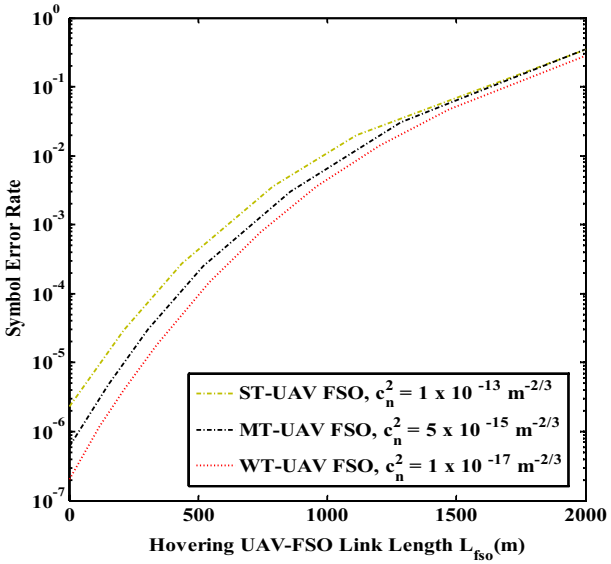

Fig. 8 SER versus UAV-FSO link length (meter), l_{fso} for different values of C_n^2 of the geometric and pointing error coefficient deviation $h_g = 0.05$ mrad

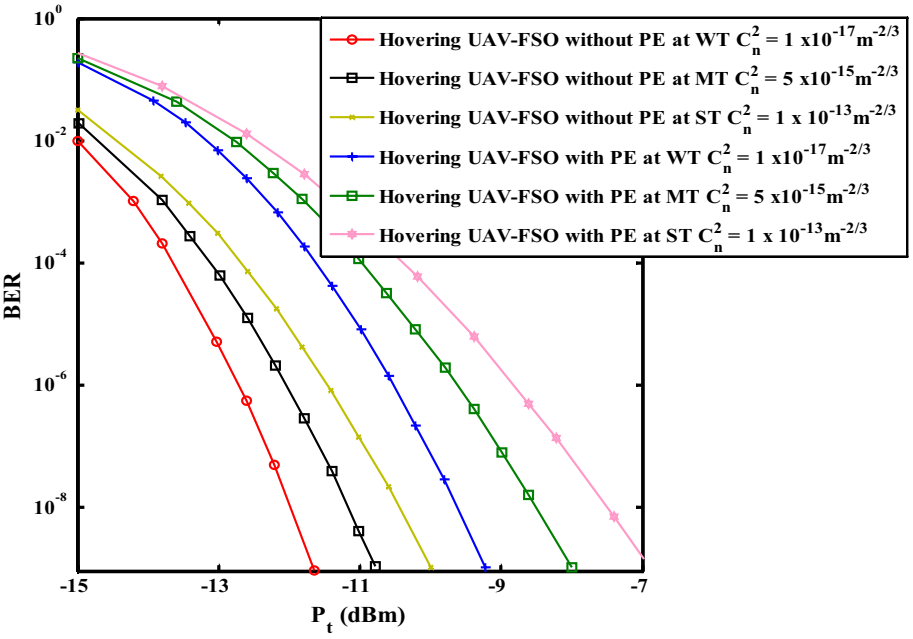

Fig. 9 Comparison between the atmospheric turbulence transmission with pointing error (PE) and without PE for BER versus the average transmitted power per symbol P_t, for different turbulence strengths $C_n^2\left(m^{-2/3}\right)$ at $l_{fso} = 2$ km

states have also been considered. The system's SER analysis was derived using multiple parameters, linking AT and the PE effect. Then, we investigated and improved the performance of the considered system's relay-assisted UAV-FSO over different channel parameters due to UAV fluctuations. The required SNR to attain a BER of 10^{-5} is 23 dB when the tilt angle of the UAVs σ_α^2 increases from 0 to 7 mrad with FSO link distance L = 2000 m. To obtain ABER of 10^{-6}, the SNR should be 16.23 dB, 17.64 dB, and 21.45 dB when σ_α^2 is 0 mrad, 1 mrad, and 2 mrad, respectively. The average BER will also increase when σ_α^2 increases. The ABER will increase from 10^{-7} to 3.38×10^{-5} at the SNR of 23 dB, when σ_α^2 increases from 0 to 7 mrad. With the ABER of 10^{-6}, the SNR should be 16.23 dB, 17.64 dB, and 21.45 dB when σ_α^2 is 0 mrad, 1 mrad, and 2 mrad, respectively. With the ABER is 10^{-5} and σ_α^2 is 5 mrad, the SNR reaches 18.77 dB while when σ_α^2 is 7 mrad, the ABER is 10^{-4} and the SNR is 10.05 dB. The SER performance improves and reaches to 10^{-11} while in the MT, the SER is at 10^{-6} and in the ST, the SER decreases to 10^{-5}. Therefore, the turbulence strength influences how well the SER performs. The OP in the CFSO of 10^{-1} while using a UAV-FSO system with four relays, the OP can reach 10^{-7}. Using relay UAV-FSO, we achieve high SNR at 20 dB at the OP of 10^{-7}. The UAV-FSO system with a UAV altitude of 250 m can reach 3.7×10^{-7} while with a UAV altitude of 500 m, achieve OP of 10^{-6}. When the UAV altitude increase, the OP increase. The UAV-FSO system performance with four stationary relays can achieve better OP and SNR. The results show the relay-assisted UAV-FSO system with five stationary relays can achieve BER 10^{-8} at 25 dB SNR in the ideal case and 10^{-5} at 27 dB SNR with AT and PE at FSO length 1000 m. The results show

the relay UAV-FSO system outperforms the CFSO at the BER and SNR performance. The effects of UAV'FSO s fluctuation increase when the UAV-FSO link length, L_{fso} increases. The results of the weak turbulence achieve better SER compared with MT and ST. The obtained results show that decreasing L_{fso} can compensate for the effects of UAV-FSO link fluctuation on the proposed system. The numerical results show that the required P_t to obtain BER of 10^{-9} are -12.7 dBm, -10.8 dBm, and -10 dBm corresponding to $C_n^2 = 1 \times 10^{-17} m^{-2/3}$, $C_n^2 = 5 \times 10^{-15} m^{-2/3}$, and $C_n^2 = 1 \times 10^{-13} m^{-2/3}$ for hovering UAV-FSO without PE, respectively. Without PE, the BER performance is significantly improved compared to in the presence of PE. The required P_t to obtain BER of 10^{-9} are -9.2 dBm, -8 dBm, and -6.8 dBm corresponding to $C_n^2 = 1 \times 10^{-17} m^{-2/3}$, $C_n^2 = 5 \times 10^{-15} m^{-2/3}$, and $C_n^2 = 1 \times 10^{-13} m^{-2/3}$ for hovering UAV-FSO with PE, respectively. The performance improvements without PE are 3.5 dB, 2.8 dB, and 3.2 dB for $C_n^2 = 1 \times 10^{-17} m^{-2/3}$, $C_n^2 = 5 \times 10^{-15} m^{-2/3}$, and $C_n^2 = 1 \times 10^{-13} m^{-2/3}$, respectively. Finally, we investigated the CFSO relay-assisted UAV-FSO system with aided NFSO-UAVs spatial diversity-based relay-based on NFSO OWC and revealed the benefits of the resulting hybrid architecture.

Author contributions All authors have made a direct and significant contribution to the manuscript. All authors reviewed the manuscript.

Funding Open access funding provided by The Science, Technology & Innovation Funding Authority (STDF) in cooperation with The Egyptian Knowledge Bank (EKB). Not applicable.

Data availability Not applicable.

Declarations

Conflict of interest The authors declare that they have no conflict of interest.

Ethical approval Not applicable.

Open Access This article is licensed under a Creative Commons Attribution 4.0 International License, which permits use, sharing, adaptation, distribution and reproduction in any medium or format, as long as you give appropriate credit to the original author(s) and the source, provide a link to the Creative Commons licence, and indicate if changes were made. The images or other third party material in this article are included in the article's Creative Commons licence, unless indicated otherwise in a credit line to the material. If material is not included in the article's Creative Commons licence and your intended use is not permitted by statutory regulation or exceeds the permitted use, you will need to obtain permission directly from the copyright holder. To view a copy of this licence, visit http://creativecommons.org/licenses/by/4.0/.

References

Ai, D.H., Trung, H.D., Tuan, D.T.: On the ASER performance of amplify-and-forward relaying MIMO/FSO systems using SC-QAM signals over lognormal and gamma-gamma atmospheric turbulence channels and pointing error impairments. J. Inf. Telecommun. **4**(3), 267–281 (2020). https://doi.org/10.1080/24751839.2020.1732734

Aladeloba, A.O., Phillips, A.J., Woolfson, M.S.: Performance evaluation of optically preamplified digital pulse position modulation turbulent free-space optical communication systems. IET Optoelectron. **6**(1), 66–74 (2012). https://doi.org/10.1049/iet-opt.2011.0029

Alzenad, M., Shakir, M.Z., Yanikomeroglu, H., Alouini, M.S.: FSO-based vertical Backhaul/Fronthaul framework for 5G+ wireless networks. IEEE Commun. Mag. **56**(1), 218–224 (2018). https://doi.org/10.1109/MCOM.2017.1600735

Andrews, L.C., Phillips, R.L.: Laser Beam Propagation through Random Media. Foreign Aff. **91**(5) (2012). http://spie.org/Publications/Book/626196?&origin_id=x113901&num_results=48&tech=5&view_as=grid

Chatterjee, M.R., Mohamed, F.H.A.: Investigation of profiled beam propagation through a turbulent layer and temporal statistics of diffracted output for a modified von Karman phase screen. Free-Space Laser Commun. Atmos. Propag. XXVI **8971**, 897102–897111 (2014). https://doi.org/10.1117/12.2033442

Ciaramella, E., Arimoto, Y., Contestabile, G., Presi, M., D'Errico, A., Guarino, V., Matsumoto, M.: 1.28 terabit/s (32×40 Gbit/s) WDM transmission system for free space optical communications. IEEE J. Sel. Areas Commun. **27**(9), 1639–1645 (2009). https://doi.org/10.1109/JSAC.2009.091213

Cruz, P.J., Fierro, R.: Towards optical wireless communications between micro unmanned aerial and ground systems. In: 2015 International Conference on Unmanned Aircraft Systems, ICUAS 2015, pp. 669–676 (2015). https://doi.org/10.1109/ICUAS.2015.7152349

Dabiri, M.T., Sadough, S.M.S., Khalighi, M.A.: Channel modeling and parameter optimization for hovering UAV-based free-space optical links. IEEE J. Sel. Areas Commun. **36**(9), 2104–2113 (2018). https://doi.org/10.1109/JSAC.2018.2864416

Dabiri, M.T., Sadough, S.M.S., Ansari, I.S.: Tractable optical channel modeling between UAVs. IEEE Trans. Veh. Technol. **68**(12), 11543–11550 (2019). https://doi.org/10.1109/TVT.2019.2940226

Dautov, K., Arzykulov, S., Nauryzbayev, G., Kizilirmak, R.C.: On the Performance of UAV-enabled Multi-hop V2V FSO systems over generalized α-μ Channels. In: Proceedings of the 2nd International Conference on Computing and Network Communications, CoCoNet 2018, pp. 69–73 (2018). https://doi.org/10.1109/CoCoNet.2018.8476910

El-Fikky, A.E.-R.A., Ghazy, A.S., Khallaf, H.S., Mahmoud Mohamed, E., Shalaby, H.M.H., Aly, M.H.: On the performance of adaptive hybrid MQAM–MPPM scheme over Nakagami and lognormal dynamic visible light communication channels. Appl. Opt. **59**(7), 1896–1906 (2020). https://doi.org/10.1364/ao.379893

El-Mottaleb, S.A.A., Métwalli, A., Hassib, M., Alfikky, A.A., Fayed, H.A., Aly, M.H.: SAC-OCDMA-FSO communication system under different weather conditions: performance enhancement. Opt. Quantum Electron. (2021). https://doi.org/10.1007/s11082-021-03269-0

Elsayed, E.E., Yousif, B.B.: Performance enhancement of M-ary pulse-position modulation for a wavelength division multiplexing free-space optical systems impaired by interchannel crosstalk, pointing error, and ASE noise. Opt. Commun. (2020). https://doi.org/10.1016/j.optcom.2020.126219

Elsayed, E.E., Yousif, B.B., Alzalabani, M.M.: Performance enhancement of the power penalty in DWDM FSO communication using DPPM and OOK modulation. Opt. Quantum Electron. (2018). https://doi.org/10.1007/s11082-018-1508-y

Elsayed, E.E., Alharbi, A.G., Singh, M., Grover, A.: Investigations on wavelength-division multiplexed fibre/FSO PON system employing DPPM scheme. Opt. Quantum Electron. (2022). https://doi.org/10.1007/s11082-022-03717-5

Fawaz, W., Abou-Rjeily, C., Assi, C.: UAV-aided cooperation for FSO communication systems. IEEE Commun. Mag. **56**(1), 70–75 (2018). https://doi.org/10.1109/MCOM.2017.1700320

Fotouhi, A., Member, S., Qiang, H., Member, S., Ding, M., Member, S., Hassan, M., Member, S., Giordano, L.G., Garcia-rodriguez, A.: Survey on UAV cellular communications: practical aspects, standardization advancements, regulation, and security challenges. IEEE Commun. Surv. Tutor. **21**(4), 3417–3442 (2019)

Ghassemlooy, Z., Popoola, W., Rajbhandari, S.: Optical wireless communications. Opt. Wirel. Commun. (2019). https://doi.org/10.1201/9781315151724

Gudimetla, V.S.R., Holmes, R.B., Farrell, T.C., Lucas, J.: Phase screen simulations of laser propagation through non-Kolmogorov atmospheric turbulence. Atmos. Propag. VIII **8038**, 77–88 (2011). https://doi.org/10.1117/12.887595

Hayal, M.R., Yousif, B.B., Azim, M.A.: Performance enhancement of DWDM-FSO optical fiber communication systems based on hybrid modulation techniques under atmospheric turbulence channel. Photonics (2021). https://doi.org/10.3390/photonics8110464

Khalighi, M.A., Uysal, M.: Survey on free space optical communication: a communication theory perspective. IEEE Commun. Surv. Tutor. **16**(4), 2231–2258 (2014). https://doi.org/10.1109/COMST.2014.2329501

Khalighi, M.A., Schwartz, N., Aitamer, N., Bourennane, S.: Fading reduction by aperture averaging and spatial diversity in optical wireless systems. J. Opt. Commun. Netw. **1**(6), 580–593 (2009). https://doi.org/10.1364/JOCN.1.000580

Kurt, G.K., Khoshkholgh, M.G., Alfattani, S., Ibrahim, A., Darwish, T.S.J., Alam, M.S., Yanikomeroglu, H., Yongacoglu, A.: A vision and framework for the high-altitude platform station (HAPS) networks of

the future. IEEE Commun. Surv. Tutor. **23**(2), 729–779 (2021). https://doi.org/10.1109/COMST.2021.3066905

Majumdar, A.K.: Free-space laser communication performance in the atmospheric channel. Free-Space Laser Commun. (2005). https://doi.org/10.1007/978-0-387-28677-8_3

Michailidis, E.T., Nomikos, N., Bithas, P., Vouyioukas, D., Kanatas, A.G.: Outage Probability of Triple-Hop Mixed RF/FSO/RF Stratospheric Communication Systems (2018). https://www.researchgate.net/publication/323602718

Najafi, M., Ajam, H., Jamali, V., Diamantoulakis, P.D., Karagiannidis, G.K., Schober, R.: Statistical modeling of the FSO Fronthaul channel for UAV-based communications. IEEE Trans. Commun. **68**(6), 3720–3736 (2020). https://doi.org/10.1109/TCOMM.2020.2981560

Trung, H.D.: Performance of UAV-to-ground FSO communications with APD and pointing errors. Appl. Syst. Innov. (2021). https://doi.org/10.3390/asi4030065

Trung, H.D., Tuan, D.T.: Performance of free-space optical communications using SC-QAM signals over strong atmospheric turbulence and pointing errors. In: 2014 IEEE 5th International Conference on Communications and Electronics, IEEE ICCE 2014, pp. 42–47 (2014). https://doi.org/10.1109/CCE.2014.6916677

Whitfield, E.M., Banerjee, P.P., Haus, J.W.: Propagation of Gaussian beams through a modified von Karman phase screen. Laser Commun. Propag. through Atmos. Oceans **8517**, 208–214 (2012). https://doi.org/10.1117/12.932277

Yousif, B.B., Elsayed, E.E.: Performance enhancement of an orbital-angular-momentum-multiplexed free-space optical link under atmospheric turbulence effects using spatial-mode multiplexing and hybrid diversity based on adaptive MIMO equalization. IEEE Access **7**, 84401–84412 (2019). https://doi.org/10.1109/ACCESS.2019.2924531

Yousif, B.B., Elsayed, E.E., Alzalabani, M.M.: Atmospheric turbulence mitigation using spatial mode multiplexing and modified pulse position modulation in hybrid RF/FSO orbital-angular-momentum multiplexed based on MIMO wireless communications system. Opt. Commun. **436**, 197–208 (2019). https://doi.org/10.1016/j.optcom.2018.12.034

Zhang, Y., Wang, Y., Deng, Y., Du, A., Liu, J.: Design of a free space optical communication system for an unmanned aerial vehicle command and control link. Photonics (2021). https://doi.org/10.3390/photonics8050163

Zheng, A., Huang, Y., Gao, S.: Modeling and spatial diversity-based receiving improvement of in-flight UAV FSO communication links. Appl. Sci. (switzerland) (2021). https://doi.org/10.3390/app11146365

Publisher's Note Springer Nature remains neutral with regard to jurisdictional claims in published maps and institutional affiliations.

Authors and Affiliations

Mohammed R. Hayal[1] · Ebrahim E. Elsayed[1] · Dhiman Kakati[2] · Mehtab Singh[3] · Abdelrahman Elfikky[4] · Ayman I. Boghdady[5] · Amit Grover[6] · Shilpa Mehta[7] · Syed Agha Hassnain Mohsan[8] · Irfan Nurhidayat[9]

✉ Ebrahim E. Elsayed
engebrahem16@gmail.com; engebrahem16@std.mans.edu.eg

Mohammed R. Hayal
mohammedraisan@gmail.com

Dhiman Kakati
dhiman.kakati@gmail.com

Mehtab Singh
mehtab91singh@gmail.com

Abdelrahman Elfikky
abdo.fikky2020@gmail.com

Ayman I. Boghdady
ayman.boghdady@aast.edu

Amit Grover
amitgrover321@gmail.com

Shilpa Mehta
shilpa.mehta@aut.ac.nz

Syed Agha Hassnain Mohsan
Hassnainagha@zju.edu.cn

[1] Department of Electronics and Communications Engineering (ECE), Faculty of Engineering, Mansoura University, Mansoura 35516, El-Dakahilia Governorate, Egypt

[2] Department of Electronics and Electrical Engineering, Indian Institute of Technology Guwahati, Guwahati, India

[3] Department of Electronics Technology, Guru Nanak Dev University, Amritsar, India

[4] Arab Academy for Science, Technology and Maritime Transport, Alexandria 1029, Egypt

[5] Port Training Institute, Arab Academy for Science, Technology and Maritime Transport, Alexandria 1029, Egypt

[6] Department of Electronics and Communication Engineering, Shaheed Bhagat Singh State University, Ferozepur, Punjab, India

[7] Department of Electrical and Electronic Engineering, Auckland University of Technology, Auckland, New Zealand

[8] Optical Communications Laboratory, Ocean College, Zhejiang University, Zheda Road 1, Zhoushan 316021, Zhejiang, China

[9] Jalan Kapur, Dusun 01, RT. 002, RW. 001, Sutawangi, Jatiwangi, Majalengka 45454, Jawa Barat, Indonesia